Publications of the Astronomical Society of the Pacific, 132:114504 (11pp), 2020 November https://doi.org/10.1088/1538-3873/abaf04

Least-squares Spectral and Wavelet Analyses of V455 Andromedae Time Series: The Life After the Super-outburst

Ebrahim Ghaderpour[1] and Shahnaz Ghaderpour[2]
[1] University of Calgary, 2500 University Drive NW, Calgary, AB T2N 1N4, Canada; ebrahim.ghaderpour@ucalgary.ca
[2] Bu-Ali Sina University, Hamedan 65178, Iran
Received 2020 July 30; accepted 2020 August 13; published 2020 October 14

Abstract

An extensive spectral analysis is performed on the light curve of dwarf nova V455 Andromedae (V455 And = HS 2331+3905) using the Least-squares WAVElet software (LSWAVE) to highlight its robustness for analyzing astronomical time series. The V455 And properties are briefly reviewed, and the recent results are compared with the results obtained herein. It is shown that the new analytical tools are superior to the traditional ones in that they consider observational uncertainties, do not require any interpolation and/or gap-filling, and can estimate the spectral peaks at a higher time–frequency resolution. First, the Anti-leakage Least-squares Spectral Analysis (ALLSSA) is applied to analyze a V455 And unequally spaced time series since 2008. ALLSSA has estimated spectral peaks at 80.40, 40.54, 1.12, and 0.56 minutes that correspond to the orbital period, its first harmonic, the white dwarf spin period, and its harmonic, respectively, confirming the earlier results. ALLSSA is then applied to all sufficiently large-size segments of the light curve to estimate the periodic components and demonstrate the double-humped orbital variations. Next, the Least-squares Wavelet Analysis (LSWA) is applied to four light curve segments each with a sufficient number of observations to study the periodic and aperiodic components. LSWA also detects the spectral peaks corresponding to the orbital period and non-radial white dwarf pulsations at a period of 4–5 minutes in 2010 October which gradually shifts toward 5–6 minutes in 2015 and 2018.

Key words: Cataclysmic variable stars – Dwarf novae – Light curves – Spectral energy distribution – Time series analysis – Wavelet analysis

Online material: color figures

1. Introduction

Accurate estimation of star system parameters, such as mass, inclination angle, orbital and spin periods, from the light curve can be very challenging due to three main factors: (1) quality and quantity of observations, (2) mathematical modeling, and (3) complexity of the system. First, the quality of observations can easily be influenced by several factors, such as telescope calibration, human error, poor weather conditions, and economy. Such factors can also make the time series unequally spaced (irregularly sampled) with long data gaps. Second, appropriate mathematical modeling for analyzing the acquired observations should consider the effect of missing observations and their uncertainties. For instance, traditional spectral analysis techniques, such as Discrete Fourier Transform (DFT) and Continuous Wavelet Transform (CWT), are not defined for unequally spaced time series, neither they consider the observational uncertainties (Mallat 1999; Mukadam et al. 2016). Thus, in order to implement these methods, one must ignore the uncertainties and make the series equally spaced by applying gap-filling and interpolation techniques that often perform poorly and can easily create significant misleading biases in the results (Vaníček 1969; Press & Teukolsky 1988). Third, the number of stars in a star system with their relative stellar sizes and masses can create complex motions (Duchene & Kraus 2013). Furthermore, the phenomena occurring among multiple stars in a star system, such as mass transfer, magnetic braking disruption, and outbursts can change the orbital and spin periods abruptly or gradually (Hameury et al. 1991; Rubinov 2004; Smith 2007; Davis et al. 2008). Thus, considering all the vibrations present in the light curve in addition to noise (random and systematic) is not an easy task.

The main goal of this research is to show that the Anti-leakage Least-squares Spectral Analysis (ALLSSA) and the Least-squares Wavelet Analysis (LSWA) can be used as alternative methods to rigorously analyze the astronomical time series[3] (Ghaderpour & Pagiatakis 2017, 2019; Ghaderpour et al. 2018). In many geophysics and geodetic applications, these methods have shown better periodicity analysis results compared to the Discrete Fourier Transform (DFT), Anti-leakage Fourier Transform (ALFT), Continuous Wavelet Transform (CWT), Least-squares spectral

[3] ALLSSA and LSWA are two of the main tools in the Least-squares WAVElet software (LSWAVE) freely available online at: https://geodesy.noaa.gov/gps-toolbox/LSWAVE.htm and https://github.com/Ghaderpour/LSWAVE-SignalProcessing.

analysis (LSSA), Hilbert–Huang Transform (HHT), Weighted Wavelet Z-Transform (WWZ), and $O-C$ method (Vaníček 1969; Lomb 1976; Foster 1996b; Mallat 1999; Sterken 2005; Xu et al. 2005; Huang & Wu 2008; Ghaderpour 2018). To show the effectiveness of the new analytical methods, V455 Andromedae (V455 And = HS 2331+3905) is selected due to its very interesting properties and widely conducted researches as described below.

First discovered in Hamburg Quasar Survey, V455 And is a dwarf nova in the Andromeda constellation (Hagen et al. 1995; Samus & Broens 2007). V455 And, classified as a cataclysmic variable, is a binary star with a white dwarf as the primary that accretes matter from the secondary donor star, orbiting around their common barycenter (Lang 2018). When the secondary star fills its Roche lobe, matter escapes from the surface through the inner Lagrange point and transfers to the white dwarf (Paczynski 1971). The masses of the white dwarf and its donor are assumed to be $0.6\,M_{\odot}$ and $0.07\,M_{\odot}$, respectively (Araujo-Betancor et al. 2005). The greater stellar mass of the white dwarf makes the barycenter closer to the center of the mass of the white dwarf.

The brightness of the system not only arises from the white dwarf, but it also arises from the accretion columns. The most significant orbital brightness variation of the system, as seen by terrestrial observers, is a double-humped continuous wave (Araujo-Betancor et al. 2005; Gänsicke 2007; Silvestri et al. 2012; Szkody et al. 2013). From the grazing eclipses, the overall inclination angle of the system, i.e., the orientation of the orbit from the observer point of view, is estimated as $i \simeq 75^{\circ}$ (Araujo-Betancor et al. 2005). The trigonometric distance between V455 And and the terrestrial observer is also estimated as 75.4 pc based on the Gaia parallax (Bailer-Jones et al. 2018).

V455 And experienced a super-outburst in 2007 September 4th, during which the brightness of the system increased by 8 mag from 16.5 to 8.5 and more than ten days after the termination of the plateau, the fading of V455 And almost stopped at 15 mag (Katysheva & Shugarov 2009; Maehara et al. 2009; Mukadam et al. 2016). The white dwarf's temperature can go beyond the instability strip during an outburst when accreting matter occurs, and the pulsations usually resume a few years after (Mukadam et al. 2016). It was estimated at around 11,100 K in 2010 that eventually cooled down to 10,600 K in 2011, and the star had a quiescent temperature of 10,500 K (Szkody et al. 2013).

The white dwarf spin period is precisely estimated as $67.61970396 \pm 0.00000072$ s that is shorter than the orbital period of approximately 81.08 minutes (Mukadam et al. 2016). The fact that the spin period is seen in the light curve suggests that a light source on or close to the surface of the spinning white dwarf exists which indirectly indicates that the white dwarf has a magnetic field, guiding matter from the accretion disk to the white dwarf poles (Mukadam et al. 2016).

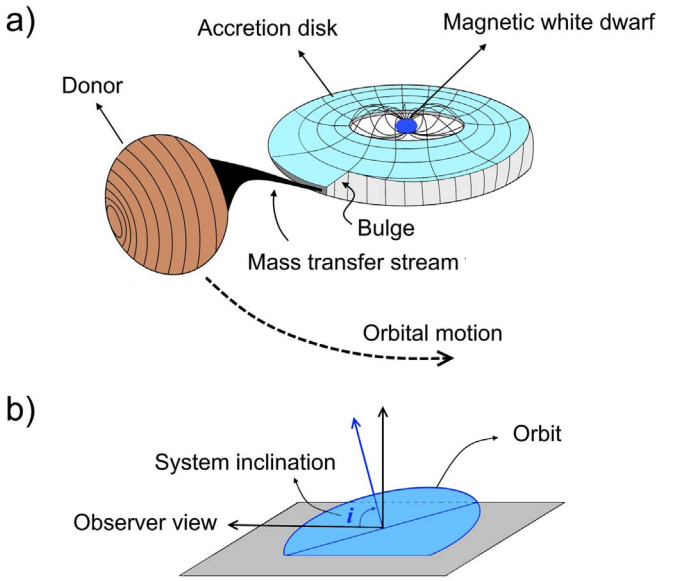

Figure 1. (a) A diagram of an intermediate polar that shows matter is flowing from the donor star into an accretion disk around the white dwarf, channeling to the white dwarf's poles due to a strong magnetic field, and (b) a diagram showing the inclination of the system orbit as seen by the terrestrial observer. (A color version of this figure is available in the online journal.)

Due to the short orbital period of V455 And, this binary star system is a unique intermediate polar (see Figure 1) with a visible white dwarf and a high-amplitude outburst, making it a very interesting cataclysmic variable for a continuous research (Szkody et al. 2013).

2. Materials and Methods

This section briefly describes the V455 And data sets, ALLSSA, and LSWA which will be applied to the data sets. The main advantages of ALLSSA and LSWA are their ability to analyze non-stationary and unequally spaced time series without any need for gap-filling and interpolation. They consider the observational uncertainties, usually in the form of a covariance matrix, to reduce the effect of noisy measurements when estimating the components. These methods simultaneously estimate the signal frequencies while considering the constituents of known forms, such as trends and sinusoids of particular frequencies.

2.1. Data Set

The V455 And data in this study are downloaded from https://www.aavso.org. The organizations affiliated with the observers that took these data are the American Association of Variable Star Observers (AAVSO), Center for Backyard Astronomy (CBA), British Astronomical Association, Variable Star Section (BAA-VSS), Variable Stars South (VSS), Royal Astronomical Society of Canada (RASC), Madrid Astronomical Association (Spain), Vereniging Voor Sterrenkunde, Werkgroep

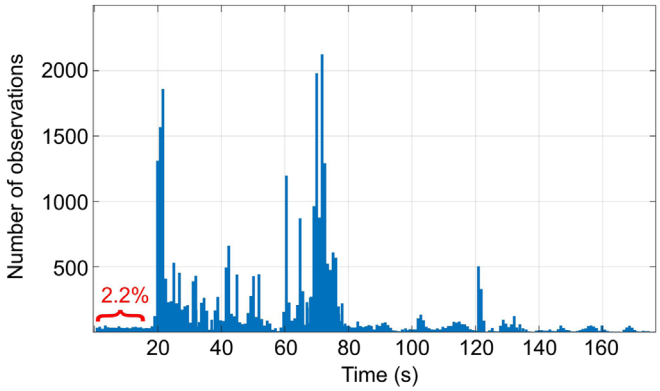

Figure 2. Histogram of the distribution of the time difference between adjacent data points in the entire V455 And time series since 2008. Only 2.2% of the observations among a total of 38,800 observations are consecutively observed shorter than 17 s to support the estimation of signals whose periods are less than 34 s without facing possible aliasing.
(A color version of this figure is available in the online journal.)

Veranderlijke Sterren (Belgium), and Association Francaise des Observateurs d'Etoiles Variables (France).

The total number of observations, including uncertainties provided by the observers, is 38,800 from 2008 January to 2020 May. The observations are reported in Julian Date without any heliocentric or barycentric corrections, see Eastman et al. (2010) for details regarding these corrections. Although disregarding such corrections may broaden any periodic signal in data sets encompassing longer intervals, it is shown that ALLSSA still detects the signals corresponding to the orbital and spin periods of V455 And for the entire 12 yr long light curve as most of the observations are provided by the observer affiliated with AAVSO. Furthermore, ignoring such corrections has no effect on the spectral and wavelet analyses of the short-duration segments presented herein as all the observations within each segment are provided by an individual observer.

The time series exhibits long gaps, and only about 50 days with a sufficient number of observations are useful for estimating the high-frequency signals corresponding to the orbital and pulsation periods without facing aliasing. Unfortunately, only a few days with data of sufficiently high time-resolution were available for estimating the spin period of the white dwarf, and so the focus here is mainly on the orbital and pulsation periods that are longer than the spin period. Figure 2 shows the distribution of the time difference between adjacent data points in the light curve as a proxy for a reliable estimation of the signals without facing possible aliasing (VanderPlas 2018; Ghaderpour 2019). Poor observational density makes the estimation of the harmonic of the white dwarf spin period less reliable which is not even possible in certain days due to aliasing. The observations are the apparent magnitudes of the star system. Herein, the spectral analysis methods are applied directly to the original observations (the apparent magnitudes).

2.2. Anti-leakage Least-squares Spectral Analysis Revisited

LSSA is a method of analyzing an unequally spaced time series which computes a spectrum by decomposing the time series into the frequency domain to investigate the periodicity and power/energy of certain components (Vaníček 1969; Lomb 1976). A spectral peak at a particular frequency in the least-squares spectrum (LSS) is obtained by fitting the sinusoids to the entire time series at that frequency (Vaníček 1969; Craymer 1998). The spectral peaks in LSS, expressed as percentage variance, show the percentage amounts that the sinusoids contribute to the time series. The critical value in LSS is derived from the normality assumption of the observations, so when the percentage variance of a spectral peak is greater than the critical value, the peak is statistically significant at a certain confidence level (usually 95% or 99%) (Ghaderpour & Pagiatakis 2017).

When a time series is unequally spaced (unevenly sampled), the sinusoids at different frequencies are generally correlated which can cause spectral leakages in the spectrum (Kovacs 1980; Foster 1996a). This means that the energy can leak from one spectral peak into another, failing to accurately estimate the frequencies, amplitudes, and phases of true signals even if a much denser set of frequencies is chosen (Chapter 3, Ghaderpour 2018). ALLSSA is based on LSSA with an improved algorithm that simultaneously estimates the periodic components as well as trends and other constituents using an iterative procedure (Ghaderpour et al. 2018). Simultaneous estimation of the components significantly attenuates the spectral leakages in the spectrum, resulting in a more accurate estimation of frequencies, amplitudes, and phases of true signals, although it can be computationally expensive for large-size time series, where size is the number of observations. For regularization purposes, ALLSSA can also prevent over/underfitting issues.

2.3. Least-squares Wavelet Analysis Revisited

When dealing with time series whose components have variability of amplitudes and frequencies over time, an appropriate time series segmentation or windowing technique must be implemented (Daubechies 1990; Foster 1996a, 1996b; Han et al. 2012). Since the fitting process in DFT, ALFT, LSSA, and ALLSSA is performed to the entire time series, the signal energy is averaged out which can be misleading. In other words, from a spectral peak in the frequency spectrum, it is not possible to determine whether the corresponding signal is short-duration (aperiodic) with large amplitude or long-duration with a small amplitude (periodic) (Ghaderpour & Pagiatakis 2017).

LSWA computes a spectrogram by decomposing a time series into the time–frequency domain, like CWT and WWZ. The segment size in LSWA is inversely proportional to the frequency, allowing the detection of both short- and long-duration signals (Ghaderpour & Pagiatakis 2019). The least-squares wavelet spectrogram (LSWS) is obtained by fitting the sinusoids to each frequency-dependent segment, expressed as percentage variance. A spectral peak in a time–frequency neighborhood in LSWS shows the percentage amount that its corresponding sinusoids contribute to the (residual) segment.

A stochastic confidence level surface can be derived from the normality assumption of observations from which the statistically significant signals can be detected. In other words, if a spectral peak in LSWS stands above the stochastic surface, then the corresponding signal is statistically significant at a certain confidence level (Ghaderpour 2018). The stochastic surface values are in fact the critical values. The critical value for each frequency-dependent segment of size n is $\zeta = 1 - \alpha^{2/(n-q-2)}$, where α is the significance level (e.g., $\alpha = 0.01$), and q is the number of constituents of known forms (e.g., $q = 2$ for linear trend) being estimated and removed from each segment while their removal effects are considered in the residual series (Ghaderpour & Pagiatakis 2017). Thus, as the segment size decreases the critical value increases, meaning that a spectral peak at higher frequencies must be taller (higher variance) to be statistically significant.

A set of weights, obtained from a Gaussian function, can be assigned to the observations within each translating window to account more for the observations toward the window center, adapting the sinusoids to the Morlet wavelet in the least-squares sense (Ghaderpour & Pagiatakis 2019). The statistical weights, i.e., the inverse-square of the observational uncertainties provided by the observer, can also be multiplied by the Gaussian function values with the recommended decay constant 0.0125 to assign appropriate weights to each frequency-dependent segment (Foster 1996b; Ghaderpour & Pagiatakis 2019). Each translating window is recommended to allow at least six cycles of sinusoids during the fitting process to compute a smooth spectrogram (Ghaderpour 2018). The statistical weights do not change the critical values, but they can significantly weaken or strengthen a spectral peak.

The amplitude-spectrogram in LSWA is obtained from the estimated sinusoidal coefficients, like the Weighted Wavelet Amplitude (WWA) (Foster 1996b). It uses the same statistical weights and shows the localized signal amplitudes, however, the stochastic surfaces are considered for the normalized spectrogram (LSWS) (Ghaderpour 2018).

3. Results and Discussion

Spectral analysis of the light curve can provide useful information for the star system. In reality, the components of the light curve corresponding to a binary star system are irregularly varying over time. The amplitudes, phases, and periods of signals for such a star system may rapidly change over time due to several factors, such as irregular non-radial pulsations, mass and angular momentum losses, and active accretion, etc. This section intents to describe how these components are changing over time using ALLSSA and LSWA.

3.1. The ALLSSA Results

For the 12 yr long time series and from Figure 2, the initial cyclic frequency range is set from 0.1 c/yr to one million c/yr which allows detecting signals whose periods are longer than 30 s. As for the constituents of known forms, the quadratic trend is selected to estimate the gradual brightness change of the system. Unlike the linear trend, the quadratic trend allows capturing the overall magnitude evolution that may be physically interpreted as the gradual cooling of the white dwarf after the super-outburst until an equilibrium level is reached.

The coefficients of the quadratic trend and all the statistically significant *periodic* components at 99% confidence level are simultaneously estimated in an iterative procedure. The time series, its regularization, and the anti-leakage amplitude spectrum are shown in Figure 3. The regularized series is obtained by adding the simultaneously estimated quadratic trend and the sinusoids given by

$$f(t) = A\sin(2\pi\omega t + \theta), \tag{1}$$

where A is amplitude, ω is cyclic frequency, t is time, and θ is the phase, some of which are listed in Table 1.

ALLSSA has estimated many statistically significant peaks at certain periods. The peaks at 40 days and 1 days with their close neighboring peaks may be explained by artifacts due to geographic locations of the observers, motion of the Earth, data quality, etc. The spectral peaks at 80.40, 40.54, 1.12, and 0.56 minutes correspond to the orbital period, its first harmonic, the white dwarf spin period, and its harmonic, respectively.

Due to the double-humped structure of the orbital modulation, the most power of the orbital period is shifted to half of the orbital period (Araujo-Betancor et al. 2005). Thus, from the strongest peak at 40.54 minutes, the orbital period may be estimated as 81.08 minutes. The period of 1.12 minutes corresponds to the spin period of the white dwarf, one of the fastest known spinning white dwarfs (Araujo-Betancor et al. 2005; Bloemen et al. 2013; Kozhevnikov 2015). The oscillations corresponding to the spin period may be physically ascribed to the changing of optical depth through the accretion curtain as the line of sight rotates, being brighter as the pole points away from the observer (Hellier et al. 1987).

The spectral peak at 5.76 minutes may correspond to the averaged-out white dwarf pulsations. The estimated quadratic trend is also in line with the evolution of the medium frequency

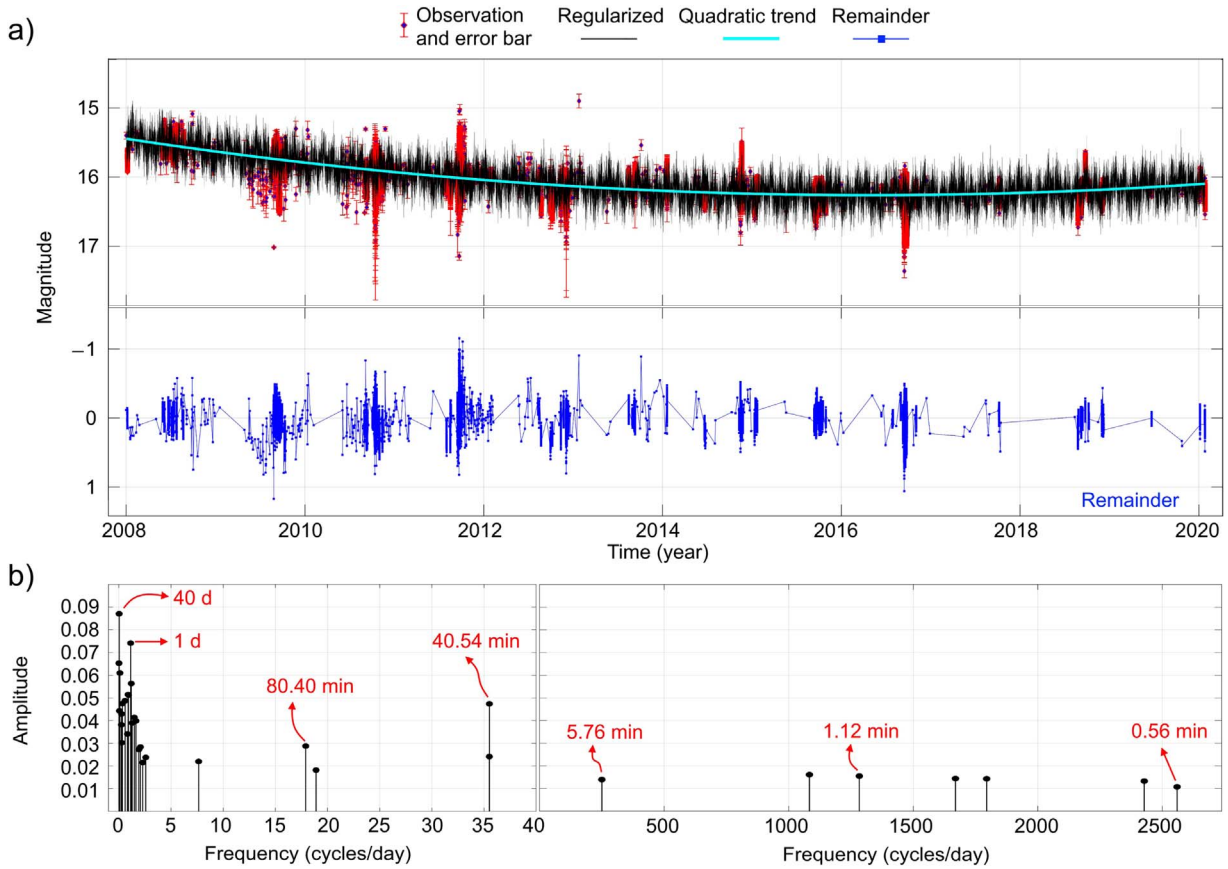

Figure 3. (a) V455 And 12 yr long time series and their ALLSSA simultaneous estimated linear trend and periodic components along with its remainder. The start day is 2008 January 2nd. (b) ALLSS of the 12 yr long time series. All the spectral peaks shown here are statistically significant at 99% confidence level. Note that the relationship between the magnitude and brightness of the star system works in reverse, i.e., the brighter the star, the smaller the magnitude.
(A color version of this figure is available in the online journal.)

Table 1
The ALLSSA Simultaneously Estimated Components of the V455 And Time Series Illustrated in Figure 3

Time Series Information		Frequency (c/d)	Period (minutes)	Amplitude	Phase (Rad)
Date	Start time (UT)	0.025	40 days	0.087 ± 0.001	0.729 ± 0.013
2008 Jan 2	01:54:31	1	1 days	0.074 ± 0.001	-0.735 ± 0.075
Length	Sample size	17.91	80.40	0.029 ± 0.001	1.169 ± 0.021
12 yr	38800	35.52	40.54	0.047 ± 0.001	-2.763 ± 0.013
Quadratic fit: $\hat{a} + \hat{b}t + \hat{c}t^2$ (t is time)		249.84	5.76	0.014 ± 0.001	-2.504 ± 0.037
$\hat{a} = 15.446 \pm 0.002$, $\hat{b} = 0.196 \pm 0.001$,		1283.43	1.12	0.016 ± 0.000	1.403 ± 0.038
$\hat{c} = -0.012 \pm 0.000$		2559.01	0.56	0.011 ± 0.001	2.536 ± 0.055

Note. Only seven main *periodic* components are listed for the 12 yr long time series. Note that the frequency is in cycles/day (c/d), and period is in minutes unless stated otherwise.

of the white dwarf pulsations as shown in Figure 3 of Bruch (2020). The linear trend was also examined separately as the constituent of known form in ALLSSA, and all the main signals listed in Table 1 were precisely estimated with some slight changes in their amplitudes and phases. Note that this analysis only provides an overall estimation for periodic (stable) signals in the entire time series and may not provide a good estimation for aperiodic signals (e.g., the pulsations).

To visualize the double-humped orbital variations over time, the estimated orbital signals of 15 well-observed nightly data sets are added to generate a fractional magnitude curve for each data set, where only two spectral peaks within 72–96 minutes

and 36–48 minutes are simultaneously estimated by ALLSSA for each data set. In other words, for each nightly data set, suppose that A_1, A_2, ω_1, ω_2, θ_1, and θ_2 are the simultaneously estimated amplitudes, cyclic frequencies, and phases of the two periodic signals corresponding to the orbital period, respectively. Each of the two signals is obtained after substituting these estimated parameters in Equation (1). Then, the two signals are added to create a factional magnitude curve, where "fractional" refers to the sum of these two signals which partially reconstructs the original light curve because other simultaneously estimated signals, as well as noise, are not added. The results are illustrated in Figure 4, where the x-axis units for the panels are fractions of the orbital period. For visualization purposes, the fractional light curve in each panel of Figure 4 starts from the time when the fractional magnitude becomes positive and ends at the orbital period (similar to a folded light curve, or phase diagram). The large-amplitude humps in the light curve arise mainly from the disk, or the hot spot on the disk (Araujo-Betancor et al. 2005; Littlefair et al. 2008).

Since the stream eclipses in magnetic cataclysmic variables are relatively unstable due to the changes in the location of the stream within the binary frame as a function of the mass transfer rate, the cause of the narrow dips observed in the light curve is likely due to the grazing eclipses of the hot spot in the accretion disk, noting that the brown dwarf companion in V455 And is not magnetically active and contributes practically no flux to the optical light from the system (Araujo-Betancor et al. 2005).

Now to demonstrate a more detailed analysis and highlight the potentials of ALLSSA and LSWA when dealing with unequally spaced time series, four segments from the 12 yr long time series are selected, exhibiting short data gaps. ALLSSA is then applied to each segment to estimate the gradual and periodic components. Table 2 shows the details of each segment along with the ALLSSA results for only the periodic components whose amplitudes are greater than 0.01. Figure 5 demonstrates each segment along with its regularization results using the estimated components, mostly listed in Table 2. The upper limit of the frequencies for each segment is determined based on the distribution of observed times to ensure that aliasing will not occur. Only on 2018 December 7th, the densely sampled data allows the reliable estimation of the white dwarf spin period, 1.12 minutes (see the last row in Table 2).

One can see from Table 2 that the first harmonic of the orbital period (which should be the strongest signal) is significantly different on 2018 December 7th. This is likely due to the quality of the observations and/or accidental

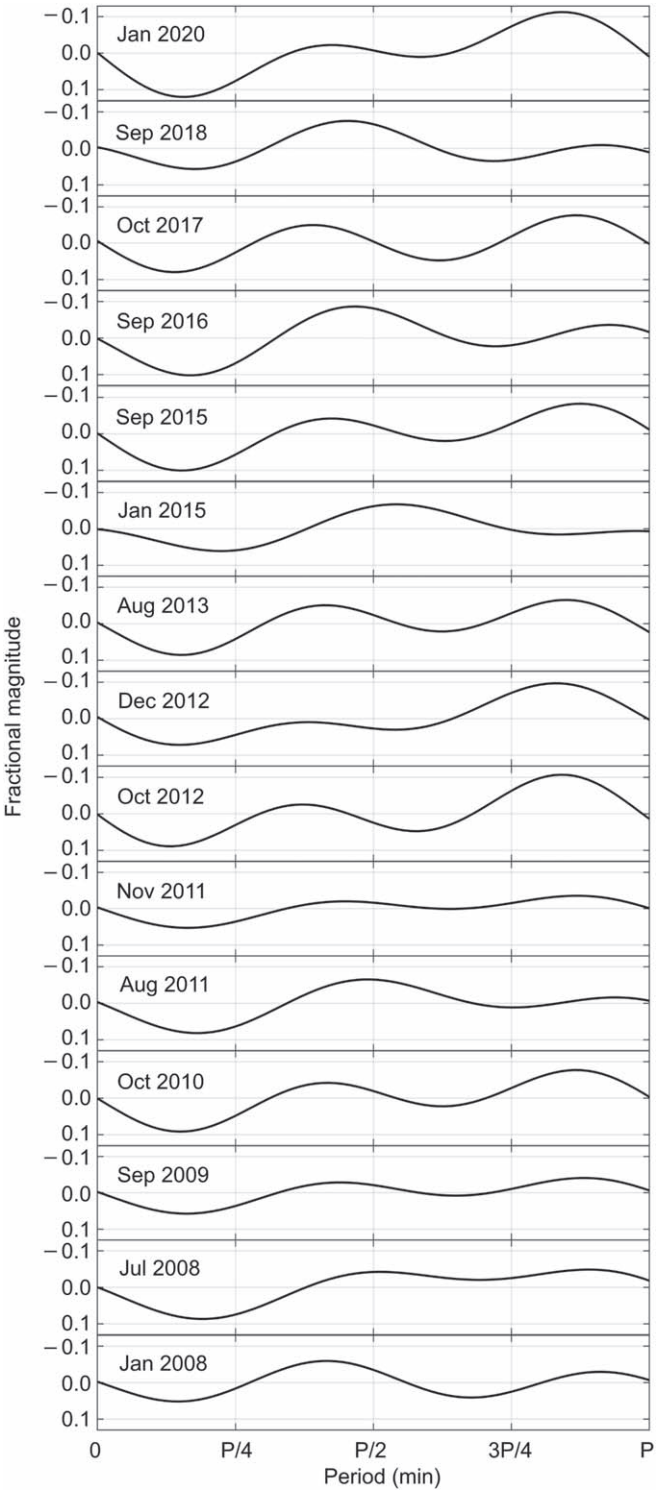

Figure 4. The fractional magnitude of the light curve obtained by adding the signals corresponding to the orbital period, where $P = 81.08$ minutes is the orbital period of the binary star system.

Table 2
The ALLSSA Simultaneously Estimated Components of the V455 And Time Series Illustrated in Figure 5

Time Series Information	Frequency (c/d)	Period (minutes)	Amplitude	Phase (Rad)
Date Start time (UT)	5.27	273.24	0.014 ± 0.002	1.813 ± 0.148
2010 Oct 6 18:57:52	11.64	123.71	0.035 ± 0.001	1.678 ± 0.054
Length Sample size	16.81	85.66	0.025 ± 0.002	−0.078 ± 2.017
5.4 hr 320	20.03	71.89	0.015 ± 0.002	−0.868 ± 0.466
Intercept Slope	35.65	40.39	0.074 ± 0.002	1.013 ± 0.030
15.814 ± 0.003 0.097 ± 0.025	46.16	31.20	0.012 ± 0.002	2.409 ± 0.157
Observer Affiliation: BAA-VSS	53.56	26.89	0.014 ± 0.002	−1.523 ± 0.013
	70.18	20.52	0.011 ± 0.002	2.430 ± 0.165
	177.57	8.11	0.012 ± 0.002	1.933 ± 0.146
	322.85	4.46	0.016 ± 0.002	1.798 ± 0.116
	330.39	4.36	0.013 ± 0.002	1.770 ± 0.140
Date Start time (UT)	4.75	303.16	0.020 ± 0.002	−2.951 ± 0.095
2015 Oct 13 02:02:29	8.39	171.63	0.012 ± 0.002	−2.889 ± 0.171
Length Sample size	18.45	78.05	0.036 ± 0.002	−0.407 ± 1.225
8.3 hr 420	35.59	40.46	0.046 ± 0.002	0.254 ± 0.054
Intercept Slope	37.23	38.68	0.012 ± 0.002	0.553 ± 0.211
16.240 ± 0.003 −0.060 ± 0.015	53.86	26.74	0.015 ± 0.002	1.823 ± 0.131
Observer Affiliation: AAVSO	71.41	20.17	0.013 ± 0.002	−2.012 ± 0.090
	243.24	5.92	0.013 ± 0.002	−2.673 ± 0.143
Date Start time (UT)	15.23	94.55	0.011 ± 0.002	1.111 ± 0.155
2018 Oct 12 05:05:45	18.57	77.54	0.032 ± 0.002	−2.911 ± 0.054
Length Sample size	35.87	40.14	0.031 ± 0.002	2.650 ± 0.058
7.5 hr 219	241.33	5.97	0.010 ± 0.002	1.990 ± 0.165
Intercept Slope				
16.142 ± 0.003 0.195 ± 0.015				
Observer Affiliation: AAVSO				
Date Start time (UT)	7.57	190.22	0.023 ± 0.003	1.805 ± 0.192
2018 Dec 7 03:33:02	19.73	72.99	0.026 ± 0.003	−0.828 ± 0.401
Length Sample size	31.28	46.04	0.030 ± 0.002	−1.459 ± 0.021
3.0 hr 494	39.24	36.70	0.015 ± 0.002	2.397 ± 0.166
Intercept Slope	107.68	13.37	0.012 ± 0.002	−2.663 ± 0.179
16.170 ± 0.006 0.026 ± 0.096	181.49	7.93	0.012 ± 0.002	−1.434 ± 0.063
Observer Affiliation: AAVSO	197.61	7.29	0.013 ± 0.002	0.963 ± 0.184
	259.75	5.54	0.025 ± 0.000	1.895 ± 0.261
	272.34	5.29	0.025 ± 0.002	3.110 ± 0.096
	282.55	5.10	0.017 ± 0.002	3.072 ± 0.145
	1286.22	1.12	0.015 ± 0.002	1.478 ± 0.157

Note. Only the periodic components whose amplitudes are greater than 0.01 are listed here.

structure in the flickering of V455 And. The non-radial pulsations at 4–5 minutes in 2010 are also shifted toward 5–6 minutes in 2015 and 2018, confirming the results in Bruch (2020). The periods 273.24, 303.16, and 190.22 minutes are comparable to the lengths of nightly light curves on 2010 October 6th, 2015 October 13th, and 2018 December 7th, respectively, and may, therefore, be artifacts of the data structure.

3.2. The LSWA Results

LSSA and LSWA are applied to the four time series segments, illustrated in Figure 5, and their LSS and LSWS results are shown in Figure 6. The spectral peaks corresponding to the first harmonic of the orbital period within the frequency range 30–40 c/d (36–48 minutes) remain stable and statistically significant over time for all the four seasons (see the colored horizontal bands in LSWS). The spectral peaks within the frequency range 15–20 c/d (72–96 minutes) in Figures 6(a) and (b) are weaker than the ones in Figure 6(c). Note that due to a higher sampling rate, the analysis of more cyclic frequencies is shown in Figure 6(d), making the orbital peaks less visible in the print version here. Interestingly, there are short-duration signals within the frequency range of 200–400 c/d (3.6–7.2 minutes) for all the four seasons, assumed to arise from the non-radial white

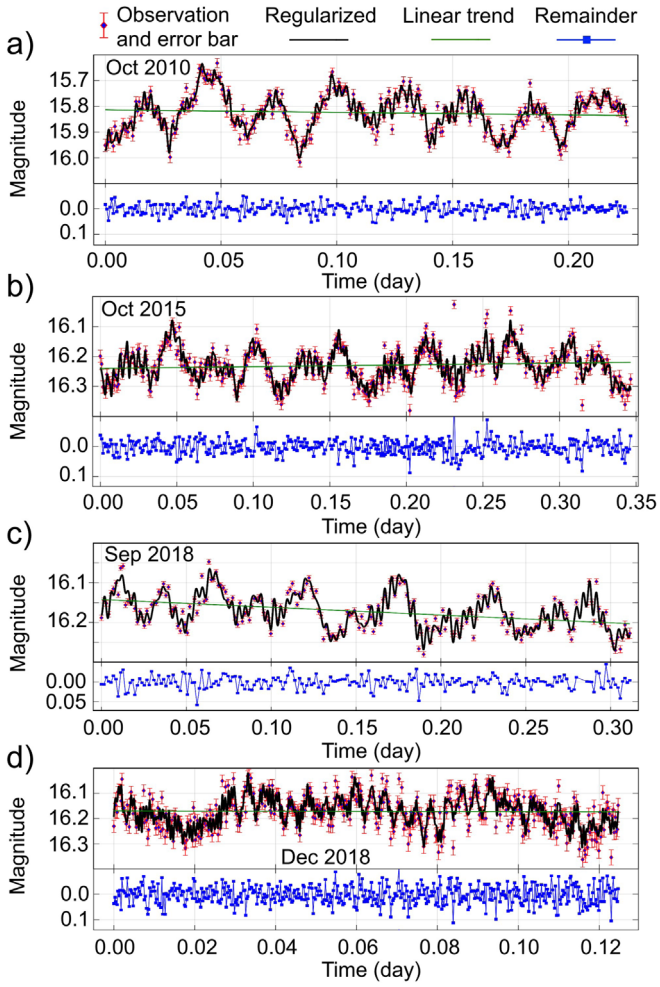

Figure 5. V455 And time series segments and their ALLSSA simultaneous estimated linear trend and periodic components along with their remainders. (A color version of this figure is available in the online journal.)

dwarf pulsations (Szkody et al. 2013). It is worth mentioning here that LSWA can resolve the spectral peaks in the time–frequency domain better than the traditional spectral analysis methods, such as CWT, LSSA, and DFT. The spectral peak at 1286 c/d (1.12 minutes) in LSS corresponds to the spin period of the white dwarf, see the peaks inside the black circle in Figure 6(d).

To investigate the signal amplitude variability over time, the ALLSSs and amplitude-spectrograms of the four time series are illustrated in Figure 7. The frequencies, periods, amplitudes, and phases of the signals whose corresponding peaks are shown in ALLSSs are listed in Table 2. From the spectrograms, one can observe the short duration signals (aperiodic) corresponding to the non-radial pulsations that are shifted from 4 to 5 minutes in 2010 toward 5–6 minutes in 2015 and 2018. Though ALLSSA could also detect these signals, the duration of these pulsations within each night cannot be seen from the spectrum as the results are only in the frequency domain not in the time–frequency domain.

The presence of short-duration signals within the frequency range 1000–1600 c/d (0.9–1.44 minutes) in the spectrograms, shown in Figures 6(d) and 7(d), may be justified by the poor quality of observations and/or the presence of noise partially from non-radial white dwarf pulsations, obscuring the spin signals, noting that the spin speed practically cannot be changing rapidly (Arras et al. 2006; Mukadam et al. 2016). Unfortunately, the aliasing does not allow such investigation for the other three seasons.

4. Conclusions

In this contribution, a comprehensive spectral analysis was successfully performed on a 12 yr long V455 And light curve (during 2008–2020, post-outburst) using LSSA, ALLSSA, and LSWA. These methods do not require evenly sampled data and can consider the observational uncertainties to improve the signal estimation. Unlike LSSA, ALLSSA can accurately estimate the periodic signals because it simultaneously estimates all statistically significant components in the time series. Like DFT, both LSSA and ALLSSA, when directly applied to the entire light curve, cannot explain the nature of the estimated signals and how the frequencies and amplitudes of components of interest are changing over time. On the other hand, LSWA, like WWZ and CWT, can determine periodic and aperiodic signals and show how the signal amplitudes and frequencies are changing over time. Aliasing, however, remains a critical issue when estimating signals at high frequencies in coarsely sampled time series. More frequent and clean observations can certainly improve the estimation of the high-frequency signals, e.g., the harmonics of the white dwarf spin period.

ALLSSA and LSWA consider the effect of trends and low-frequency signals (e.g., arisen from the gradual cooling of the star, motion of the Earth, etc.) when estimating the signals of interest. This can potentially attenuate noise so that the signals of interest can be detected and estimated more accurately. For short-time segments, such low-frequency signals can be approximately modeled by applying a linear or quadratic trend as the initial constituents of known forms. The spectral and wavelet results presented herein confirm the previous results in Szkody et al. (2013), Mukadam et al. (2016), Bruch (2020):

1. The brightness of V455 And is gradually fading since 2008, mainly due to the gradual cooling of the white dwarf and the hot spot on the accretion disk and/or lower mass transfer, until an equilibrium level is reached. The long-term evolution of the system brightness as shown herein has not explicitly been mentioned in the literature.
2. The orbital period of the system is approximately 81.08 minutes, and the spectral peaks at a period of

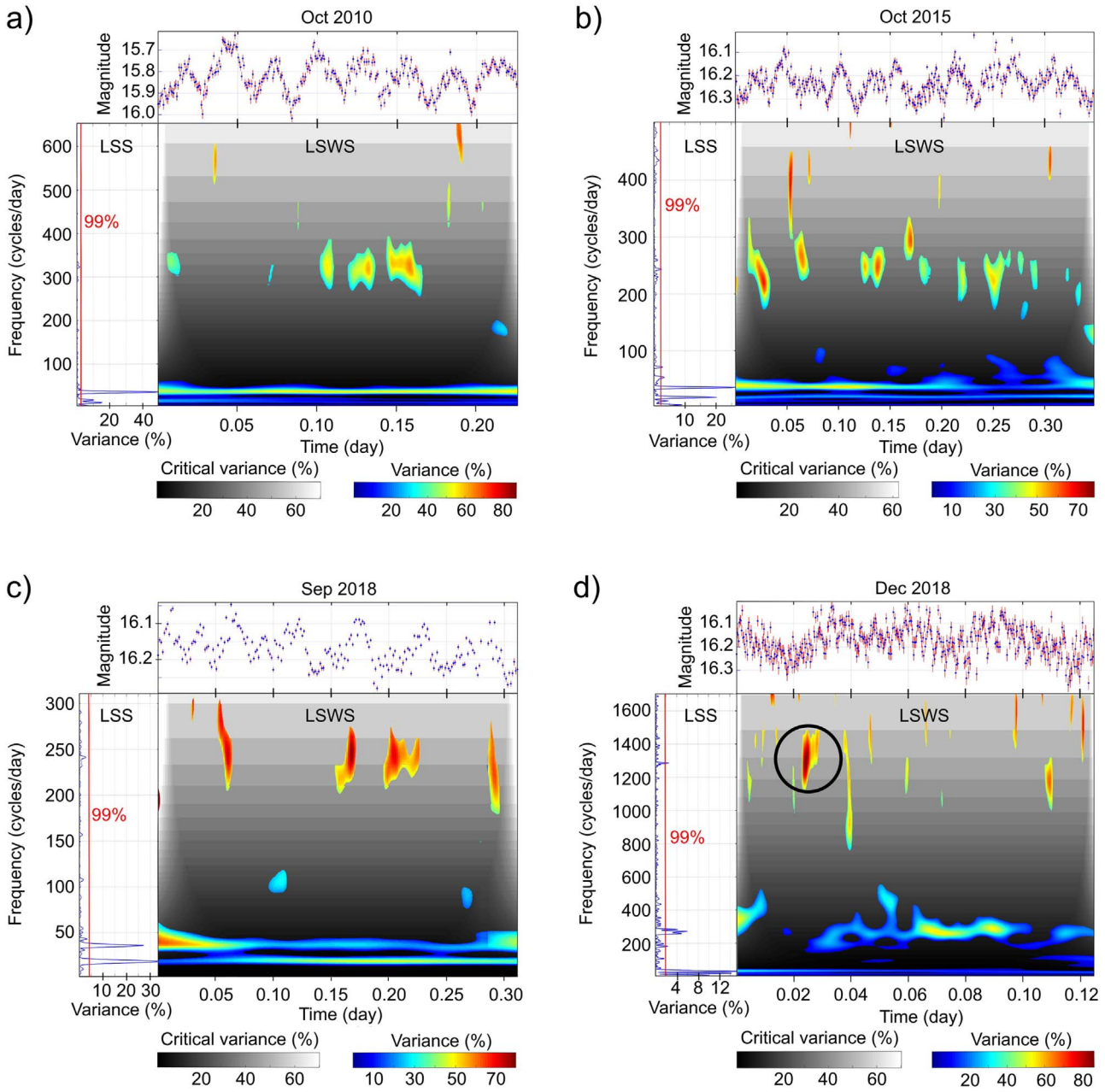

Figure 6. Four V455 And light curve segments with their LSSA and LSWA results at 99% confidence level. The percentage critical values in LSS and LSWS are displayed by red lines and gray surfaces, respectively. The peaks inside the black circle in panel (d) likely correspond to the white dwarf spin period. The reader is referred to Ghaderpour & Pagiatakis (2017, Figure 9) for a 3D visualization example.
(A color version of this figure is available in the online journal.)

4–5 minutes in 2010 October correspond to the non-radial white dwarf pulsations, gradually shifted toward 5–6 minutes in 2015 and 2018.

3. The spin period of 1.12 minutes is estimated in 2018 December, almost the same as the average estimate for the entire light curve since 2008.

The spectral analysis methods used herein can be applied to more densely sampled time series for monitoring the spin period of the white dwarf more rigorously than the traditional methods, such as DFT and $O - C$ method. We encourage the use of ALLSSA and LSWA for the followup investigation on cataclysmic variables including V455 And for better

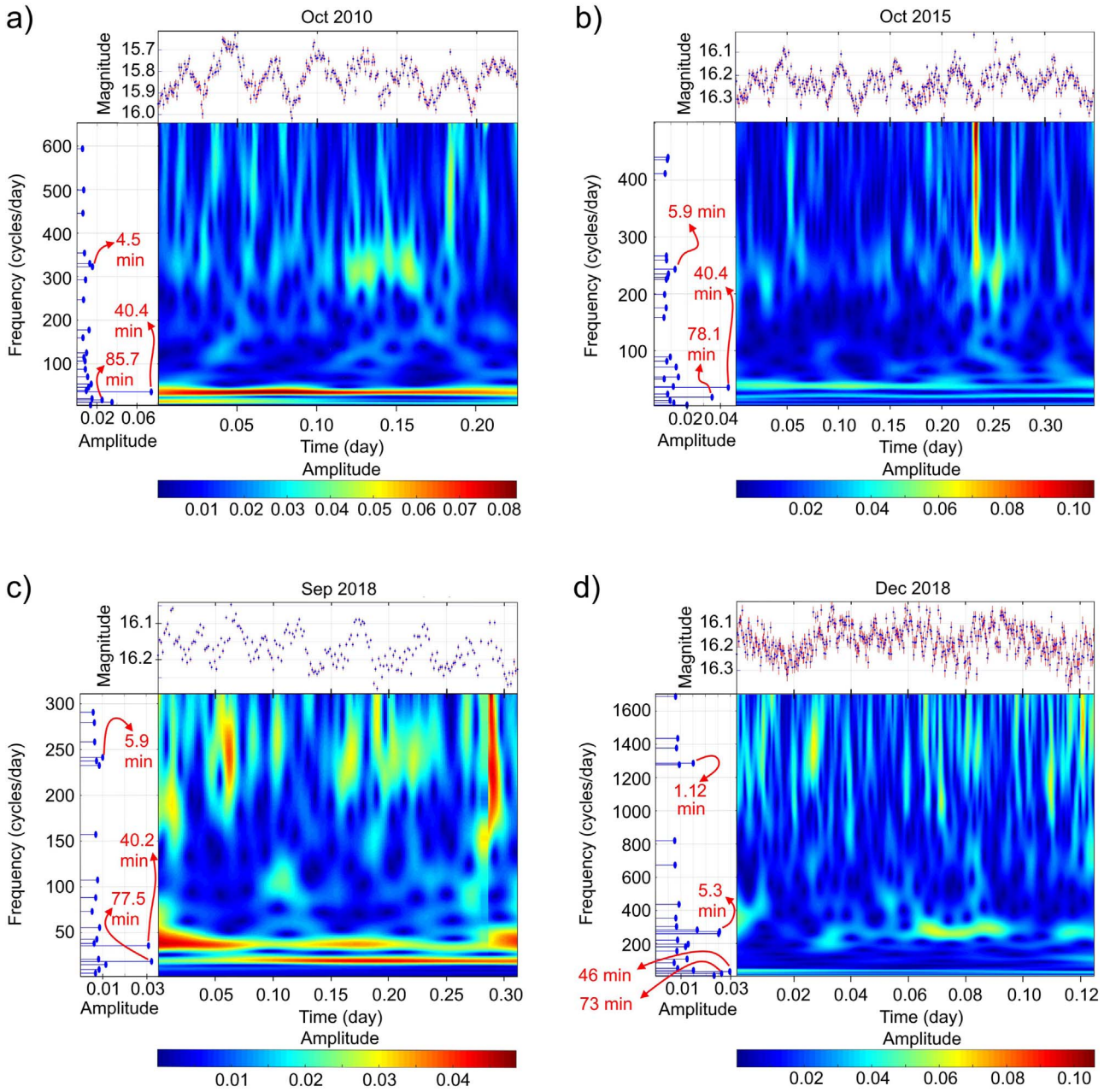

Figure 7. Four V455 And light curve segments, same as the ones shown in Figures 5 and 6, with their ALLSSA and LSWA results. The left panels are ALLSSs, and the right panels are amplitude-spectrograms. The orbital and pulsation periods are shown in red arrows.
(A color version of this figure is available in the online journal.)

understanding of the pulsations and accretion effects on the white dwarfs. These robust signal estimators can help to find solutions for many unsolved puzzles in astronomy and astrophysics.

The authors acknowledge with thanks the AAVSO scientists and associated personnel for providing the data sets used in this research. The authors also thank Drs. Paula Szkody and Allen Shafter and the anonymous reviewer for their comprehensive comments that significantly improved the presentation of the paper.

ORCID iDs

Ebrahim Ghaderpour https://orcid.org/0000-0002-5165-1773

References

Araujo-Betancor, S., Gänsicke, B. T., Hagen, H. J., et al. 2005, A&A, 430, 629
Arras, P., Townsley, D. M., & Bildsten, L. 2006, AJ, 643, L119
Bailer-Jones, C. A. L., Rybizki, J., Fouesneau, M., Mantelet, G., & Andrae, R. 2018, AJ, 156, 58
Bloemen, S., Steeghs, D., De Smedt, K., et al. 2013, MNRAS, 429, 3433
Bruch, A. 2020, NewA, 78, 101369
Craymer, M. R. 1998, PhD thesis, Univ. Toronto
Daubechies, I. 1990, ITIT, 36, 961
Davis, P. J., Kolb, U., Willems, B., & Gänsicke, B. T. 2008, MNRAS, 389, 1563
Duchene, G., & Kraus, A. 2013, ARA&A, 51, 269
Eastman, J., Siverd, R., & Gaudi, B. S. 2010, PASP, 122, 935
Foster, G. 1996a, AJ, 111, 541
Foster, G. 1996b, AJ, 112, 1709
Gänsicke, B. T. 2007, in ASP Conf. Ser. 372, The 15th European Workshop on White Dwarfs, ed. R. Napiwotzki & M. R. Burleigh (San Francisco, CA: ASP), 597
Ghaderpour, E. 2018, PhD thesis, York Univ.
Ghaderpour, E. 2019, AcGeo, 67, 1349
Ghaderpour, E., Liao, W., & Lamoureux, M. P. 2018, Geop, 8, V157
Ghaderpour, E., & Pagiatakis, S. D. 2017, Math. Geosci., 49, 819
Ghaderpour, E., & Pagiatakis, S. D. 2019, GPS Solut., 23, 50
Hagen, H. J., Groote, D., Engels, D., & Reimers, D. 1995, A&AS, 111, 195
Hameury, J. M., King, A. R., & Lasota, J. P. 1991, A&A, 248, 525
Han, X., Wang, J., Lin, J., & An, T. 2012, in Wireless Communications, Networking and Mobile Computing (WiCOM) (Piscataway, NJ: IEEE) (https://doi.org/10.1109/WiCOM.2012.6478616)
Hellier, C., Mason, K. O., Rosen, S. R., & Cordova, F. A. 1987, MNRAS, 228, 463
Huang, N. E., & Wu, Z. 2008, RvGeo, 46, RG2006
Katysheva, N., & Shugarov, S. 2009, J. Phys. Conf. Ser., 172, 012044
Kovacs, G. 1980, Ap&SS, 69, 485
Kozhevnikov, V. P. 2015, NewA, 41, 59
Lang, K. R. 2018, A Brief History of Astronomy and Astrophysics (Singapore: World Scientific)
Littlefair, S. P., Dhillon, V. S., Marsh, T. R., et al. 2008, MNRAS, 388, 1582
Lomb, N. R. 1976, Ap&SS, 39, 447
Maehara, H., Imada, A., Kubota, K., et al. 2009, in ASP Conf. Ser. 404, The 8th Pacific Rim Conf. on Stellar Astrophysics: A Tribute to Kam-Ching Leung, ed. B. Soonthornthum (San Francisco, CA: ASP), 57
Mallat, S. 1999, A Wavelet Tour of Signal Processing (Cambridge: Academic), 637
Mukadam, A. S., Pyrzas, S., Townsley, D. M., et al. 2016, ApJ, 821, 14
Paczynski, B. 1971, ARA&A, 9, 183
Press, W. H., & Teukolsky, A. 1988, CIP, 2, 77
Rubinov, A. V. 2004, ARep, 48, 45
Samus, N. N., & Broens, E. 2007, IAC Circular, 8868, 2
Silvestri, N. M., Szkody, P., Mukadam, A. S., et al. 2012, AJ, 144, 84
Smith, R. C. 2007, ConPh, 47, 363
Sterken, C. 2005, in ASP Conf. Ser. 335, The Light-Time Effect in Astrophysics, ed. C. Sterken (San Francisco, CA: ASP), 3
Szkody, P., Mukadam, A. S., Gänsicke, B. T., et al. 2013, ApJ, 775, 66
VanderPlas, J. T. 2018, ApJS, 236, 16
Vaníček, P. 1969, Ap&SS, 4, 387
Xu, S., Zhang, Y., Pham, D., & Lambare, G. 2005, Geop, 70, V87